

Soft Matter

Accepted Manuscript



This is an *Accepted Manuscript*, which has been through the Royal Society of Chemistry peer review process and has been accepted for publication.

Accepted Manuscripts are published online shortly after acceptance, before technical editing, formatting and proof reading. Using this free service, authors can make their results available to the community, in citable form, before we publish the edited article. We will replace this *Accepted Manuscript* with the edited and formatted *Advance Article* as soon as it is available.

You can find more information about *Accepted Manuscripts* in the [Information for Authors](#).

Please note that technical editing may introduce minor changes to the text and/or graphics, which may alter content. The journal's standard [Terms & Conditions](#) and the [Ethical guidelines](#) still apply. In no event shall the Royal Society of Chemistry be held responsible for any errors or omissions in this *Accepted Manuscript* or any consequences arising from the use of any information it contains.

Effect of external electric fields on the phase behavior of colloidal silica rods

Anke Kuijk,^a Thomas Troppenz,^b Laura Filion,^a Arnout Imhof,^a René van Roij,^b Marjolein Dijkstra,^a and Alfons van Blaaderen^a

Received Xth XXXXXXXXXXXX 20XX, Accepted Xth XXXXXXXXXXXX 20XX

First published on the web Xth XXXXXXXXXXXX 200X

DOI: 10.1039/b000000x

We examine the effect of external electric fields on the behavior of colloidal silica rods. We find that the electric fields can be used to induce para-nematic and para-smectic phases, and to reduce the number of defects in smectic phases. At high field strengths, a new crystal structure was observed that consisted of strings of rods ordered in a hexagonal pattern in which neighboring rods were shifted along their length. We also present a simple model to describe this system, which we used in computer simulations to calculate the phase diagram for rods of $L/D = 6$, with L the end-to-end length of the rods and D the diameter of the rods. Our theoretical predictions for the phase behavior agree well with the experimental observations.

1 Introduction

Colloidal self-assembly is a promising route for the design and fabrication of novel, advanced functional materials. For many applications, the ability to control the properties of colloidal suspensions is essential. Such control can be exerted in a variety of ways, e.g. by changing the properties of the solvent such that the interactions between the constituent particles are tuned, by applying external fields such as electric and magnetic fields, and by shearing the sample, see for example Refs. ¹⁻⁴. In particular, electric fields have been shown to change the structural, rheological, dielectric and optical properties of colloidal suspensions. ^{2,5,6} Recently, several groups have come to the conclusion that the use of electric and magnetic fields is necessary to achieve equilibrium structures for more complex particles (for examples see: Refs. ⁶⁻⁸) and/or to achieve completely new structures that could not be realized without such fields (e.g., Refs. ^{6,9-11}). Understanding the behavior of colloids in electric fields is thus important to modify material properties in a controlled way. In this paper we examine both experimentally and theoretically the effect of electric fields on the phase behaviour of colloidal rod suspensions.

When colloidal particles are placed in an external E-field, the induced polarization of the particles leads to both alignment of the particles with the field and dipole-dipole interactions between the particles. To date, experimental studies of colloids in electric fields have mainly focused on

spheres^{2,12-14} with some recent studies on anisotropic particles such as ellipsoids and dimers.^{7,15,16} With respect to rods, Kang *et al.* studied concentrated dispersions of the *fd*-virus in electric fields;¹⁷⁻¹⁹ this group also contributed to the theoretical understanding of rods in external fields by considering the electric field induced ion distribution around the rods.²⁰ The phase behaviour of rods in electric fields was also examined using computer simulations²¹ where the induced dipole moment that spherocylinders obtain in an electric field was modeled by two charges placed at the ends of the cylindrical part of the particle. In this study, the authors predicted a new crystal phase where the rods were aligned with the field, with hexagonal ordering in the plane perpendicular to the field, but staggered in the field direction by 1/3 of the length of the rods, which corresponds to their diameter, with respect to their neighbours.

The current study takes advantage of the recent development of a new monodisperse colloidal system of rods^{22,23} which makes it possible to study, for the first time, concentrated dispersions on the single particle level. Using this system, we study the effect of electric fields on the phase behavior of rods in both dilute and concentrated suspensions for a variety of aspect ratios from $L/D = 3.6$ to 6.0 , where L is the end-to-end length of the rods and D is the diameter. Note that this definition of L is slightly different from the one usually used in theoretical papers²⁴⁻²⁶ where it normally indicates the length of only the cylindrical part of the spherocylinder. The reason is that the experimental particles are not perfect spherocylinders. We use high frequency fields in this work to exclude the contributions of the electric double layers and ion fluxes to the polarizability, leaving only dielectric polarization of the particle itself and not the double layer. We compare the phase

^a Soft Condensed Matter, Debye Institute for Nanomaterials Science, Department of Physics and Astronomy, Utrecht University, Princetonplein 5, 3584 CC Utrecht, The Netherlands; E-mail: A.vanBlaaderen@uu.nl

^b Institute for Theoretical Physics, Utrecht University, Leuvenlaan 4, 3584 CE Utrecht, The Netherlands

behaviour we observed experimentally for rods with aspect ratio $L/D = 6.0$ to a phase diagram determined from computer simulations.

This paper is organized as follows: in section II we describe a model for colloidal rods in an external field, in section III we describe our experimental methods, in section IV we describe our experimental results and compare our results for rods of length $L/D = 6$ to simulation results.

2 Model

We model the rods as hard, parallel, polarizable spherocylinders in a solvent with dielectric constant ϵ_{sol} . Similar to Ref.²¹, we place two charges, q and $-q$, located a distance δ_z from the centers of the spherical hemispheres (see Fig. 1), in order to model the polarization of the rods. As the induced dipole in this model is represented by two charges, we refer to this as a double charge model. The pairwise potential between the spherocylinders is then given by

$$\beta U(\mathbf{r}) = \begin{cases} \beta U_{\text{dip}}(\mathbf{r}), & \text{if the rods do not overlap} \\ \infty, & \text{if the rods overlap} \end{cases} \quad (1)$$

where

$$\beta U_{\text{dip}}(\mathbf{r}) = \gamma \left(\frac{2D}{r} - \frac{D}{\sqrt{r_{\perp}^2 + (r_{\parallel} + L - D + 2\delta_z)^2}} - \frac{D}{\sqrt{r_{\perp}^2 + (r_{\parallel} - L + D - 2\delta_z)^2}} \right), \quad (2)$$

with r the length of \mathbf{r} , r_{\perp} and r_{\parallel} denoting the distances between the centers of the spherocylinders in the direction perpendicular and parallel to the field, $\beta = \frac{1}{k_B T}$, k_B the Boltzmann constant, T the temperature, and

$$\gamma = \frac{\beta q^2}{4\pi\epsilon_{\text{sol}}D}. \quad (3)$$

The charge q can be related to an applied electric field E by equating the dipole moment of a rod in the double charge model to that of a rod composed of a polarizable material of dielectric constant ϵ_{rod} which is polarized uniformly along the direction of the external field. We find

$$q = \left(\frac{\alpha}{L - D + 2\delta_z} \right) E \quad (4)$$

where the rod polarizability α is determined from the Clausius Mossotti relation and

$$\alpha = 3v_{\text{rod}}\epsilon_{\text{sol}} \left(\frac{\epsilon_{\text{rod}} - \epsilon_{\text{sol}}}{\epsilon_{\text{rod}} + 2\epsilon_{\text{sol}}} \right) \quad (5)$$

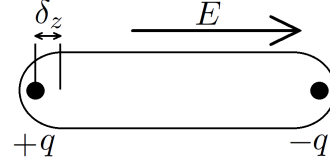


Fig. 1 Model of a single rod in the double charge approximation. Note that δ_z is the distance between the charge and the center of the spherical hemisphere on the end of the spherocylinder.

with v_{rod} the volume of the rod. The only model parameter not defined by the experimental setup is δ_z . In order to determine this parameter, we compared the pair potential energy of the double charge model U for various values of δ_z to a system where the rods were approximated by ~ 6100 permanent dipoles arranged on a simple cubic lattice.²⁷ For $L/D = 6$, this resulted in a choice of $\delta_z/D = 0.276$.

3 Experimental Methods

3.1 Dispersions

The fluorescent rods were prepared as described in Refs.^{22,23}. The particles produced by this synthesis are bullet-shaped, i.e. a cylinder with one rounded end and one flat end. The systems that were used to study the rods in an electric field are listed in Table 1. Systems B35 and B31 consisted of non-fluorescent core particles with a 30 nm fluoresceine isothiocyanate (FITC) labeled fluorescent inner shell and a 190 nm non-fluorescent outer shell. Systems N51 and B48 had a rhodamine isothiocyanate (RITC) labeled core and a 150 nm and 175 nm non-fluorescent shell, respectively. B48 and N51 had a fluorescent pattern that faded from the rounded to the flat end.

The solvent mixture consisted of dimethylsulfoxide (DMSO, $\geq 99.9\%$, Sigma-Aldrich) and ultrapure water (Milipore system). The particles were dispersed in DMSO first, after which water was added until the refractive index was matched by eye. This resulted in a 10/0.85 volume ratio of DMSO/water with an index of refraction of 1.47 and a viscosity of 1.92 cP (at 20°C). The system is not density-matched. Therefore, the rods sediment, which leads to the formation of liquid crystalline phases at the bottom of the cell.

3.2 Sample cells

Three types of sample cells were used (see Fig. 2): one to apply a field directed perpendicular to gravity (to align the rods in the phases they form due to gravity) and two sample cells to apply a field directed parallel to gravity (to study the phases that are formed when gravity is counteracted by an electric field). The first consisted of two 50 μm diameter T2 thermocouple alloy wires (Goodfellow) running on opposite sides

	L (μm)	σ_L	D (nm)	σ_D	L/D	V (μm^3)
B35	3.3	10%	550	11%	6.0	0.74
B31	2.37	10%	640	7.5%	3.6	0.69
B48	2.6	8.5%	630	6.3%	4.0	0.7
N51	2.66	10%	530	6.3%	5.0	0.55

Table 1 Dimensions of the systems of rods as measured by transmission electron microscopy (TEM). Here, L is the end-to-end length of the rods, D the diameter of the rods, $\sigma_{L(D)}$ the polydispersity in the length (diameter) of the rods, and V the volume of the rods.

through a 0.1×1 mm glass capillary (Fig. 2a). The distance between the wires was around 0.7 mm. The capillaries were sealed with a layer of candle wax, followed by a layer of two-component epoxy (Bison).

For the experiments with a relatively low electric field parallel to gravity, 0.1×1 mm capillaries were used, with glass walls of 0.1 mm thick, that were coated with 3 nm of chromium and 7 nm of gold, subsequently (Fig. 2b). The capillary was positioned on top of two $50 \mu\text{m}$ wires to keep it horizontal; one of these served as an electrical contact and was connected with a standard electronic wire. A second contact was made by placing a $50 \mu\text{m}$ wire on top of the capillary, connecting it to the capillary by silverpaint (SPI-paint) and wrapping it around a standard electronic wire. The same type of cell was used for the experiments with dilute systems in an electric field. In this case the two gold-coated sides of a square 0.2×0.2 mm capillary were placed on the side, so that an electric field perpendicular to gravity was created.

A high electric field, parallel to gravity, was applied using cells that consisted of two conductive and transparent indium tin oxide (ITO) coated glass slides (30-60 Ω , Diamond Coatings Ltd), which were separated by glass spacers (No. 00 cover slips by Menzel-Gläser, thickness around $100 \mu\text{m}$), see Fig. 2c. The conductive sides of the ITO-slides were on the inside of the cell, in direct contact with the dispersion, and all parts were glued together with UV-glue (Norland No. 68). Electrical contacts were made by gluing $50 \mu\text{m}$ diameter wires to the conductive side of the ITO slides with silverpaint. The thin electrical wires were wrapped around standard electronic wires to enable connection to the electrical set-up. The cells were sealed with UV-glue.

For configurations in which several layers of material are positioned between the electrodes, which is the case when the electrodes are on the outside of the capillary, the electric field inside any of these layers can be calculated by:

$$E_i = \frac{V}{\epsilon_i} \left(\frac{\epsilon_1 \epsilon_2 \epsilon_3}{d_1 \epsilon_2 \epsilon_3 + d_2 \epsilon_1 \epsilon_3 + d_3 \epsilon_1 \epsilon_2} \right), \quad (6)$$

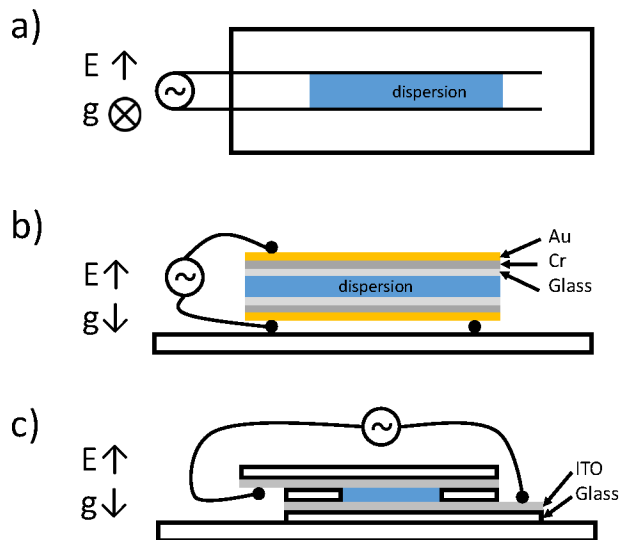


Fig. 2 Schematic representation of the used sample cells. a) Field perpendicular to gravity. b-c) Field parallel to gravity.

with V the applied voltage, ϵ_i the dielectric constant of the material the field strength is calculated in, ϵ_{1-3} the dielectric constants of layers 1-3 and d_{1-3} the thickness of layer 1-3. When the electrodes are in direct contact with the solvent E is simply V/d (d the distance between the electrodes).

3.3 Observations in an electric field

A function generator (Agilent, type 33220A or 33120A) was used to generate a sinusoidal signal with a frequency of 1 MHz and an amplitude of 3.0 V. The generated signal was sent to the sample via a wide band amplifier (Krohn-Hite, 7602M), which was used to control the field strength in the sample cell. The field strength was measured by an oscilloscope (Tektronix, TDS3012B or TDS3052) and is given in the effective root mean square (RMS) value ($V_{RMS}/\mu\text{m}$) in this paper. Observations of the phase behavior were done with a Leica TCS SP2 confocal microscope with a $63\times$ or $100\times$ oil immersion objective.

4 Results and discussion

4.1 Dilute dispersions of polarizable rods in electric fields.

When an electric field is applied to silica particles that are dispersed in a mixture of DMSO and water, the relatively high contrast in dielectric constant between the colloid ($\epsilon_{SiO_2} \sim 4.5\epsilon_0$)²⁸ and the solvent ($\epsilon_{DMSO/water} \sim 50\epsilon_0$) induces a dipole

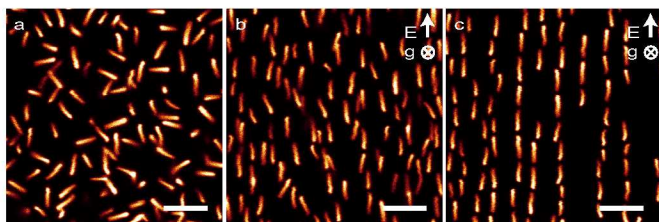


Fig. 3 Dilute dispersions of $L/D = 5$ rods (N51) in a 1 MHz electric field. (a) Rods oriented in random directions when no field was applied. (b) Rods oriented along the field direction formed a para-nematic phase at low field-strengths ($E \sim 0.05 \text{ V}/\mu\text{m}$). (c) At higher field-strengths ($E \sim 0.1 \text{ V}/\mu\text{m}$) rods oriented head-to-toe in strings due to dipole-dipole interactions. Scale bars indicate $5 \mu\text{m}$.

moment in each rod. For rods, the strength of the dipole moment depends on the orientation of the particle with respect to the field direction. Furthermore, the behavior of rod-like particles in an electric field depends on the strength of their dipole moments, which can be influenced by changing the strength of the applied external electric field. In our experiments we used an electric field with a frequency of 1 MHz to prevent polarization of the double layer. The behavior of a dilute dispersion of rods at different electric field strength regimes is shown in Fig. 3. While the rods were randomly oriented when no electric field was applied, they oriented with their long axis parallel to the field direction at low field strength ($E \sim 0.05 \text{ V}/\mu\text{m}$). When the field was increased to $E \sim 0.1 \text{ V}/\mu\text{m}$, string formation was observed, in agreement with the behaviour seen in systems of spheres subjected to an E-field.^{2,12–14}

4.2 Concentrated dispersions of short rods in low electric fields.

We studied concentrated dispersions of “short” rods with an aspect ratio of $L/D = 3.6$. Outside the presence of an electric field, these short rods crystallize directly from the isotropic phase into hexagonally ordered domains that are primarily single layers without regular stacking.²⁹ These rods are too short to form nematic or smectic liquid crystal phases, as was already predicted by computer simulations on hard spherocylinders.²⁶ However, with the application of electric fields we have a tool at our disposal to induce and control orientational order in this system of sedimenting rods. The formation of a para-nematic phase was trivial in this case: the rods aligned when a field of $0.05 \text{ V}/\mu\text{m}$ was applied and a para-nematic phase was formed (similar to that shown in Fig. 3b for $L/D = 5$). We noticed that the field needed to align particles in the concentrated sediment of a sample was lower than the field needed to align rods in the dilute top-part of a sample. In a field of $0.03 \text{ V}/\mu\text{m}$, sediments aligned, while the top-part showed an isotropic phase that aligned at a field of

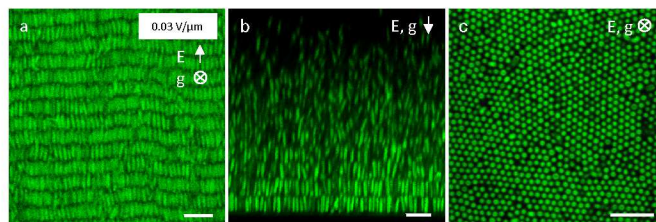


Fig. 4 Short $L/D = 3.6$ rods (B31) after sedimentation in a $0.03 \text{ V}/\mu\text{m}$ electric field, starting from a volume fraction of 0.1 in a $100 \mu\text{m}$ high capillary formed a para-smectic phase. (a) Electric field perpendicular to gravity: the rods aligned with the field and formed layers. (b) Electric field parallel to gravity: the rods aligned with the field and ordered in layers. (c) Within the layers, the rods showed hexagonal ordering (second layer from the bottom). Scale bars indicate $5 \mu\text{m}$.

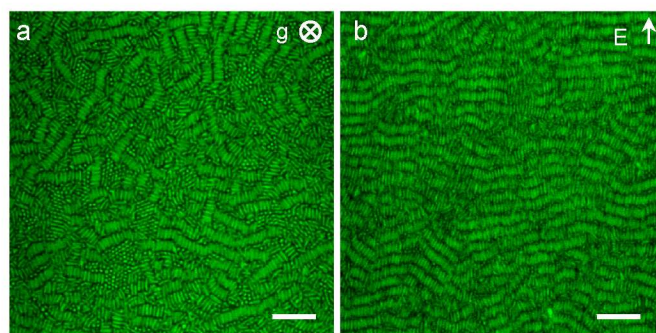


Fig. 5 Short $L/D = 3.6$ rods after sedimentation. (a) Without application of an external electric field. (b) Two days after a $0.03 \text{ V}/\mu\text{m}$ electric field had been switched off. Scale bars indicate $10 \mu\text{m}$.

$0.05 \text{ V}/\mu\text{m}$. This effect can be explained by the fact that in the dilute phase, alignment is caused only by the interaction between the induced dipole and the field. In the sediment, however, nematic order is already favored by the higher density which means that a lower electric field is required to align the rods.

Interestingly, it was found that the combination of the induced orientational order caused by the field and the increase in density due to sedimentation resulted in the formation of a regularly layered structure as shown in Fig. 4. Within the layers, the rods showed hexagonal ordering, but no positional correlation was found between neighboring layers. Therefore, the structure was identified as a smectic- B phase. These para-smectic phases were only found in the presence of an electric field for such short rods.

When the field was increased to $0.07 \text{ V}/\mu\text{m}$, dipole-dipole interactions started to contribute significantly, leading to a repulsive interaction between the ends of neighboring rods. This resulted in a distortion of the layered structure and a transition, to a crystal structure in which the rods are positioned on a

hexagonal lattice in the plane perpendicular to the E-field, and shifted in the field direction. Because this structure is more easily visualized with long rods, it will be discussed including images in the next section.

The structured smectic and crystal phases that short rods formed under the influence of an electric field were not stable when the field was turned off. After turning a $0.07 \text{ V}/\mu\text{m}$ off, the system went from an induced crystal phase to a smectic phase similar to the one shown in Fig 4a, which subsequently relaxed in the same way as a para-smectic. Figure 5b shows that a para-smectic that had been formed by applying a $0.03 \text{ V}/\mu\text{m}$ field, relaxed back to a state with considerably less order than the smectic within two days, but with still more order than a system that had not been exposed to an electric field at all (Fig. 5a).

4.3 Concentrated dispersions of long rods in low electric fields.

In contrast to the short rods, particles with an aspect ratio of $L/D = 6$ exhibit nematic and smectic liquid crystal phases when they sediment, even without an external electric field.²⁹ While an electric field was not needed to induce orientational order, we found it to be helpful in controlling the direction of alignment and in reducing defects. In particular, we observed alignment of particles in the sediment parallel to the field for electric fields of $0.02 \text{ V}/\mu\text{m}$. In agreement with the experiments on shorter rods, a layered structure with rods pointing in the field direction was formed when the field was applied during sedimentation. Additionally, this behaviour could also be induced by applying the field after the rods had sedimented. In this case the rods rotated to align with the field within 20 minutes and the sample rearranged resulting in a single domain with only one orientation (Fig. 6b), in contrast to the multiple domains present before the applied field (Fig. 6a). The Fourier transforms of the images, also depicted in Fig. 6, clearly show that the order increases when a field is applied. When the electric field was switched off after 1 night, the general orientation of the rods remained in the (former) field direction, but several defects were formed (Fig. 6c). A possible explanation for the formation of defects is provided by the inter-layer spacing. In a field of $0.02 \text{ V}/\mu\text{m}$, the inter-layer spacing was $1.24 L$, which decreased to $1.16 L$ when the field strength was zero. This difference can be associated with the weak dipole-dipole interactions, which caused the ends of the rods in one layer to repel each other slightly. As a result, the rods shift in position with respect to their neighbors and stick out partly above or below the layer, making it effectively broader. When the field is turned off, dipole-dipole interactions disappear and the system relaxes back to its original inter-layer spacing. However, since there was more space between the layers when the field was on, this allowed for de-

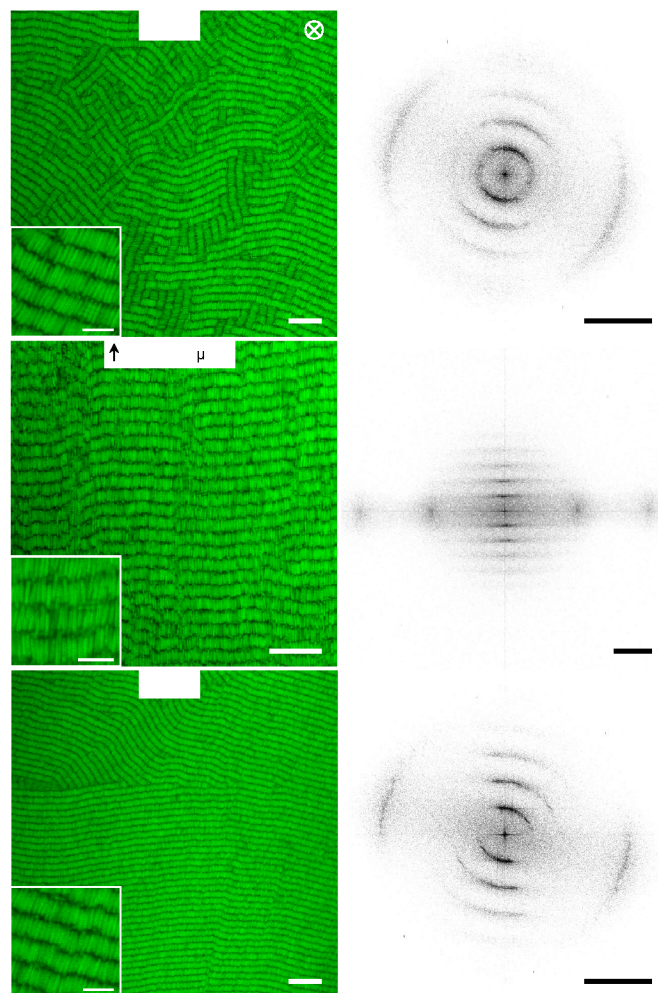


Fig. 6 Applying a field to a sediment of $L/D = 6$ rods, the initial volume fraction was 0.05 in a $100 \mu\text{m}$ high capillary. The images were taken at different positions in the sample, but at approximately the same height (a few microns from the bottom). (a) After 1 night of sedimentation without electric field. (b) 30 minutes after turning on a $0.02 \text{ V}/\mu\text{m}$ field. (c) 5 days after the field had been turned off. (d-f) Fourier transforms on a logarithmic intensity scale of the images on the left. Scale bars indicate $15 \mu\text{m}$ for a-c, $5 \mu\text{m}$ for the insets and $3 \mu\text{m}^{-1}$ for d-f.

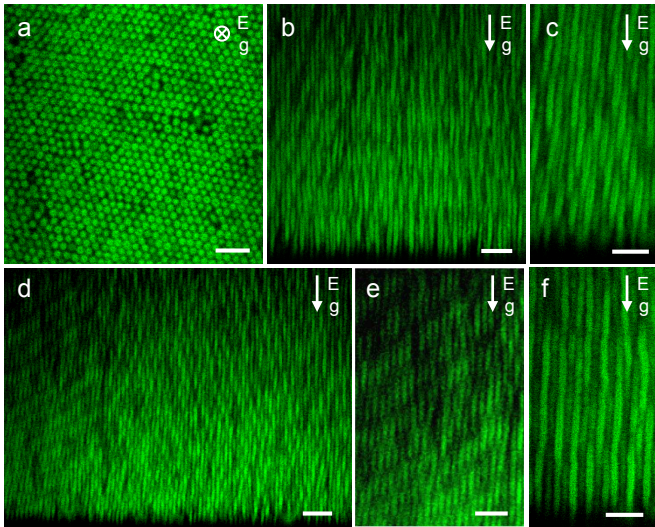


Fig. 7 Long $L/D = 6$ rods in a $0.06 \text{ V}/\mu\text{m}$ field parallel to gravity. (a) Hexagonal ordering in the xy -direction. (b and d) Overview of crystal planes parallel to the field direction. (c-f) Close-ups of different planes of the same crystal parallel to the field direction. (c) Plane in which rods are shifted one third of their length up or down with respect to their neighbors. (e) Plane in which neighboring rods are shifted one sixth of their length. Scale bars indicate $5 \mu\text{m}$ for a,d and $3 \mu\text{m}$ for b,c,e,f.

fects to form. Figure 6c shows that these defects are mainly splay distortions and edge dislocations.

In fields higher than $0.03 \text{ V}/\mu\text{m}$ (up to $0.14 \text{ V}/\mu\text{m}$), the interaction induced by the electric field increased to the point where ordering into layers was no longer favorable. However, the hexagonal ordering in the radial direction remained (Fig. 7a). In this field strength regime, it was energetically most favorable to shift neighboring rods up or down along their length. The resulting configuration of rods is a crystal structure where the rods are aligned in columns parallel to the electric field, and the columns are hexagonally ordered. Additionally, the columns are staggered with respect to each other by an integer multiple of $L/6$ (Fig. 7b-f). This is not commensurate with the C_3 -symmetric crystal structure found in computer simulations by Rotunno *et al.* for rods of $L/D = 3$ in an external electric field.²¹ However, the crystal we found as well as the crystal identified by Rotunno *et al.* consisted of hexagonally ordered chains of rods shifted integer multiples of the diameter with respect to each other. Similar structures have been reported for spherical colloids in electric fields,^{12,30} which also show string formation and form staggered crystals (body centered tetragonal (BCT) structure). The symmetry, however, is different: BCT has a tetragonal symmetry, while the crystal structure of the rods in electric fields is hexagonal.

We further explored the phase behavior of rods of length $L/D = 6$ in an external electric field using computer simu-

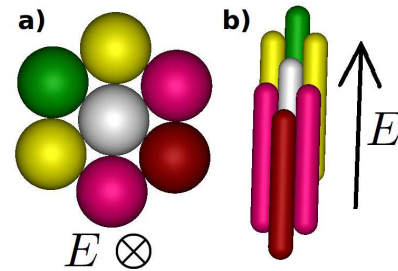


Fig. 8 a) and b) correspond to various representations of crystal X. Note that the rods are shifted along their length by $L/6$.

lations. In particular, we determined the phase diagram for $N = 864$, $L/D = 6$ model spherocylinders in an electric field using Monte Carlo simulations in combination with full free-energy calculations³¹ and common tangent constructions. The resulting phase diagram is shown in Figure 9. As shown in Figure 9, we find regions of stability for nematic, smectic, columnar, and various crystalline phases (ABC, AAA, HSC and X). Note that the crystalline phase ABC(AAA) corresponds to hexagonal layers of rods which have an ABC(AAA) stacking, while the X crystal phase consists of rods aligned into columns, where the columns are hexagonally arranged and staggered with respect to each other as shown in Figure 8. The hexagonal smectic C (HSC) phase is similar to the smectic C phase, but with rods in the layers ordered hexagonally. The angle between the long axis of the spherocylinders and the layers found in the smectic C and HSC phases was highly variable. The region on the phase diagram labeled AAA/HSC displays complicated phase behavior: when the field is turned off, the system exhibits purely the AAA phase but for weak interaction strengths, the system shifts between AAA and HSC. Finally, at sufficiently high interaction strength, the columnar phase takes over. The phase behaviour for zero field agrees with the previous computer simulation studies of parallel hard spherocylinders.^{24,25} When we compare the predicted phase diagram to our experimental results, we find strong agreement. In particular, crystal X is consistent with the planes depicted in Figure 7, and the nematic and smectic phases appear in both simulations and experiment. More details on the double charge model and the phase diagram will be published separately.²⁷

4.4 Rods in high electric fields

At field-strengths higher than $0.14 \text{ V}/\mu\text{m}$, dipole-dipole interactions became so strong that the rods formed strings from the bottom upwards rather than sedimenting to the bottom of the sample, as shown in Fig. 10 for rods with $L = 2.6 \mu\text{m}$ and $D = 630 \text{ nm}$, i.e. $L/D = 4$. Together with string formation, voids appeared in the xy -plane, and the rods grouped together

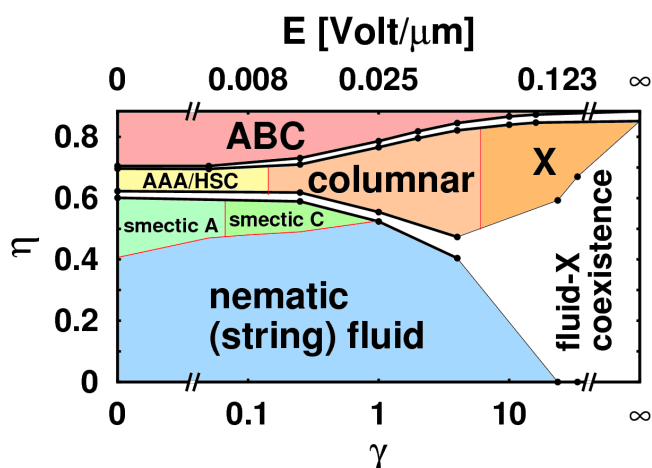


Fig. 9 Phase diagram for parallel, polarizable $L/D = 6$ spherocylinders in the double charge model.

in time (Fig. 10a-b). In contrast to spheres in high fields,¹² the rods did not form sheets in fields of $0.18 \text{ V}/\mu\text{m}$. It is not certain at this moment if this is true for all volume fractions. Since dipoles placed side-by-side are repulsive, the sideways attraction can only be favorable if the rods are shifted along their length. Indeed, the groups of rods slowly ordered into a crystal structure. At higher field strengths ($0.25 \text{ V}/\mu\text{m}$), the formation of a crystal structure occurred faster due to stronger interactions. Figure 10d shows that eventually all rods became part of the crystal columns. Unfortunately, we did not succeed in applying electric fields higher than $\sim 0.25 \text{ V}/\mu\text{m}$ in sample cells with an electrode gap of $120 \mu\text{m}$. At higher fields, temperature differences caused flow in the sample. Attempts to prevent this included the coating of the electrodes with a thin (100 nm) layer of silica to prevent any current running through the sample. Also, a glycerol/water mixture and DMSO without water were tried as a solvent. However, none of these were successful.

5 Conclusions

In conclusion, individual rods were aligned and liquid crystal phases were formed at high concentrations by applying electric fields with strengths less than $0.03 \text{ V}/\mu\text{m}$. For short rods ($L/D = 3.6$) at higher volume fractions, the induced orientational order caused by the electric field led to the formation of para-nematic and -smectic phases that would not have formed without the application of an electric field. Long rods ($L/D = 6$) that do spontaneously form equilibrium nematic and smectic phases were forced to orient in one direction, which led to the formation of a smectic phase with only one orientation throughout the sample. The application of the electric field additionally decreased the number of defects in

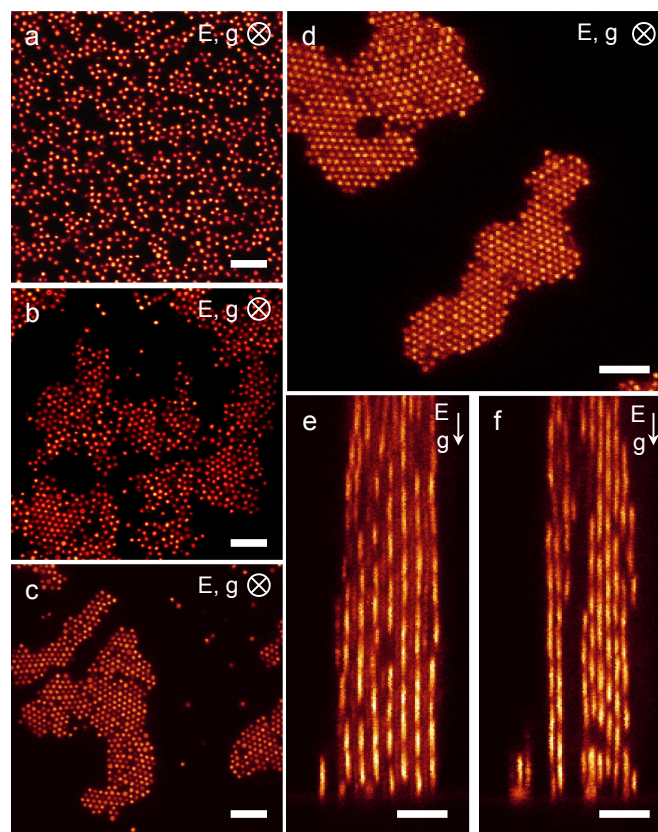


Fig. 10 Short $L/D = 4$ rods in a field parallel to gravity, $10 \mu\text{m}$ above the bottom. Gap width is $\sim 120 \mu\text{m}$. (a) 1.5 min after switching a $0.18 \text{ V}/\mu\text{m}$, 1 MHz field on. (b) 18 min after the field was turned on. (c) Increasing the field to $0.25 \text{ V}/\mu\text{m}$. (d) A few minutes later. (e) Side-view of the sample showing the crystalline structure of the columns. (f) Cut through the crystal showing an $L/3$ jump in z -position of neighboring rods. Scale bars indicate $5 \mu\text{m}$.

smectic phases of long rods significantly. Also, the nematic phase was extended to lower volume fractions under the influence of an electric field. The combination of an electric field between 0.03 and 0.14 V/ μm and an increased volume fraction due to sedimentation caused the formation of crystals in both the long and short rods. In the case of the long rods, in this structure the particles are aligned into columns which are further hexagonally arranged, and the columns are staggered with respect to each other by $L/6n$, where n is an integer. The staggered arrangement occurs in order to minimize the unfavorable “side-by-side” dipole-dipole interactions. Fields higher than 0.14 V/ μm were found to induce string formation so strongly that sedimentation was counteracted. When the field was pointing in the same direction as gravity and at large gap widths, columns of tightly packed rods were formed that again showed crystalline order. Finally, the phase behaviour we observed experimentally was well captured by Monte Carlo simulations of the double charge model which we employed to describe the polarizable rods in an E-field.

6 Acknowledgements

This work is part of the D-ITP consortium and part of the DFG/FOM program SFB-TR6 (project B8), programs of the Netherlands Organisation for Scientific Research (NWO) that is funded by the Dutch Ministry of Education, Culture and Science (OCW).

References

- I. Cohen, T. G. Mason and D. A. Weitz, *Phys. Rev. Lett.*, 2004, **93**, year.
- A. Yethiraj and A. van Blaaderen, *Nature*, 2003, **421**, 513–517.
- T.-j. Chen, R. N. Zitter and R. Tao, *Phys. Rev. Lett.*, 1992, **68**, 2555–2558.
- M. E. Leunissen, H. R. Vutukuri and A. van Blaaderen, *Adv. Mater.*, 2009, **21**, 3116–3120.
- A. Gast and C. Zukoski, *Adv. Colloid Interface Sci.*, 1989, **30**, 153.
- A. van Blaaderen, M. Dijkstra, R. van Roij, A. Imhof, M. Kamp, B. W. Kwaadgras, T. Vissers and B. Liu, *Eur. Phys. J. Special Topics*, 2013, **222**, 2895–2909.
- A. F. Demirörs, P. M. Johnson, C. M. van Kats, A. van Blaaderen and A. Imhof, *Langmuir*, 2010, **26**, 14466–14471.
- J. W. Swan, J. L. Bauer, Y. Liu and E. M. Furst, *Soft Matter*, 2014, **10**, 1102–1109.
- B. Liu, T. H. Besseling, M. Hermes, A. F. Demirörs, A. Imhof and A. van Blaaderen, *Nature Communications*, 2014, **5**, 3092.
- K. Chaudhary, J. J. Juárez, Q. Chen, S. Granick and J. A. Lewis, *Soft Matter*, 2014, **10**, 1320.
- A. Yethiraj, A. Wouterse, B. Groh and A. van Blaaderen, *Phys. Rev. Lett.*, 2004, **92**, 058301.
- U. Dassanayake, S. Fraden and A. van Blaaderen, *J. Chem. Phys.*, 2000, **112**, 3851–3858.
- A. P. Hynninen and M. Dijkstra, *Phys. Rev. Lett.*, 2005, **94**, 138303.
- A. P. Hynninen and M. Dijkstra, *Phys. Rev. E*, 2005, **72**, 051402.
- M. Mittal and E. M. Furst, *Adv. Funct. Mater.*, 2009, **19**, 3271–3278.
- J. D. Forster, J. G. Park, M. Mittal, H. Noh, C. F. Schreck, C. S. O’Hern, H. Cao, E. M. Furst and E. R. Dufresne, *ACS Nano*, 2011, **5**, 6695–6700.
- K. Kang, *Europhys. Lett.*, 2010, **92**, 18002.
- K. Kang and J. K. G. Dhont, *Europhys. Lett.*, 2008, **84**, 14005.
- K. Kang and J. K. G. Dhont, *Soft Matter*, 2010, **6**, 273–286.
- J. K. G. Dhont and K. Kang, *Eur. Phys. J. E*, 2010, **33**, 51–68.
- M. Rotunno, T. Bellini, Y. Lansac and M. A. Glaser, *J. Chem. Phys.*, 2004, **121**, 5541–5549.
- A. Kuijk, A. van Blaaderen and A. Imhof, *J. Am. Chem. Soc.*, 2011, **133**, 2346–2349.
- A. Kuijk, A. Imhof, M. H. W. Verkuijlen, T. H. Besseling, E. R. H. van Eck and A. van Blaaderen, *Part. Part. Syst. Charact.*, 2014.
- J. A. C. Veerman and D. Frenkel, *Phys. Rev. A*, 1991, **43**, 4334–4343.
- D. Frenkel, H. N. W. Lekkerkerker and A. Stroobants, *Nature*, 1988, **332**, 822–823.
- P. G. Bolhuis and D. Frenkel, *J. Chem Phys.*, 1997, **106**, 666.
- T. Troppenz, L. Fillion, M. Dijkstra and R. van Roij, to be submitted 2014.
- CRC Handbook of Chemistry and Physics*, CRC Press, 92nd edn., 2011.
- A. Kuijk, D. V. Byelov, A. V. Pethukov, A. van Blaaderen and A. Imhof, *Farad. Discuss.*, 2012, **159**, 181 – 199.
- R. Tao and J. M. Sun, *Phys. Rev. Lett.*, 1991, **67**, 398–401.
- D. Frenkel and B. Smit, *Understanding Molecular Simulation: From Algorithms to Applications*, Elsevier Science, 2001.

Graphical abstract:
(20-30 words)

We investigate, using experiments and computer simulations, the behavior of colloidal rods in external electric fields. We find stable para-nematic, para-smectic and crystalline phases.

